Carbon Trends 5 (2021) 100084

Contents lists available at ScienceDirect

Carbon Trends

journal homepage: www.elsevier.com/locate/cartre

Rational description and modelling of the separation of nanotubes from solid nanoparticles in centrifugation processes

José Carlos Ciria[a], Alejandro Ansón-Casaos[b,*], Ana M. Benito[b], Wolfgang K. Maser[b]

[a] Departamento de Informática e Ingeniería de Sistemas, Universidad de Zaragoza, María de Luna 1, 50018 Zaragoza, Spain
[b] Instituto de Carboquímica, ICB-CSIC, Miguel Luesma Castán 4, 50018 Zaragoza, Spain

ARTICLE INFO

Article history:
Received 31 March 2021
Revised 11 June 2021
Accepted 6 July 2021

Keywords:
Carbon nanostructures
Aspect ratio
Particle size distribution
Selective centrifugation
Purification
Theoretical modelling

ABSTRACT

Centrifugation of liquid dispersions is a typical technique being employed to separate single-walled carbon nanotubes (SWCNTs) from big aggregates and impurities. Shining light on the underlying mechanism contributes to a more efficient preparation of corresponding suspensions or inks with improved properties. In this work, we model the sedimentation process by applying fundamental equations and a mathematical algorithm for the centrifugation routine, which takes into account centrifugation parameters and the geometry of nanoparticles. The model is fed with experimental data, namely, the centrifugation mass yield, the SWCNT purity index, metal contents, and nanoparticle sizes measured for pristine, thermally-oxidized, and chemically functionalized SWCNT samples. Particle aggregation, including SWCNT bundling, and changes due to physicochemical pretreatments are taken into account. It is shown that the complete experimental data set can be quantitatively well understood in terms of the particle sedimentation coefficient. The proposed model thus provides a rational concept to optimize centrifugation protocols for the separation of mixtures containing nanoparticles of different shapes.

1. Introduction

Carbon nanotubes (CNTs) are usually synthesized as solid powders and then processed in the liquid phase. Organic solvents and surfactant solutions are typical base fluids for the dispersion of the hydrophobic CNTs. Selective sedimentation by centrifugation is an effective method for conditioning CNT dispersions. Indeed, the literature widely describes how metal impurities and large carbon aggregates, including CNT bundles, are quite easily separated from individual CNTs at low spin velocities. However, a high yield removal of small-sized nanoparticles, as well as encapsulated and attached impurities, is hard to achieve. On the other hand, a definite understanding of how selective separation proceeds is still lacking.

Centrifugation techniques have enabled great advances in CNT science, particularly in single-walled carbon nanotubes (SWCNTs). Centrifugation in surfactants, as well as subsequent stages of oxidation and centrifugation, were described years ago as a part of protocols for the purification of SWCNTs [1–4]. Besides, it was shown that high-speed centrifugation (ultracentrifugation) provides a high ratio of individualized SWCNTs in the dispersions [5,6]. Density gradient ultracentrifugation is used for sorting SWCNTs with different lengths or electronic characteristics: semiconducting, metallic, and even samples with a selected chirality [7–14]. Analytical ultracentrifugation has been successfully applied to the determination of the length distribution of SWCNT samples and dimensions of the SWCNT solvation sphere, as well as to elucidate the configuration of surfactant molecules around dispersed SWCNTs [15–20]. In particular, those experiments have provided abundant information concerning the application of sedimentation theories to SWCNTs. Besides, centrifugation theories have been quite extensively applied and developed for size selection in graphene oxide dispersions and other 2D materials [21–24].

The present article does not focus on CNT sorting, nor on analytical techniques, but on preparative centrifugation as a way to separate nanotubes from nanoparticle impurities, which will be modelled as spheres of distinct sizes. In previous works, X-ray diffraction analysis demonstrated that graphite particles can be separated from SWCNTs at relatively low spin velocities [25]. Moreover, it was shown that a pre-treatment by air oxidation leads to improved purity levels at low spin velocities, while a reflux in oxidant acids and a reductive treatment with hydrogen were not effective [26]. Thus, it was suggested that certain oxygen functional groups might contribute to the selective stabilization of SWCNTs in

* Corresponding author.
E-mail address: alanson@icb.csic.es (A. Ansón-Casaos).

https://doi.org/10.1016/j.cartre.2021.100084

the liquid [27]. Later, it was observed that high levels of purity can be achieved by ultracentrifugation at spin velocities of higher than 120,000 $\times g$, even starting from SWCNTs with a variety of chemical functional groups [27]. The comprehensive interpretation of those results is still lacking.

In this article, the theory of centrifugation is applied to the selective sedimentation of SWCNTs and it is reconciled with the effects of different oxidation and chemical functionalization processes on SWCNTs. A logical method is developed to compute and quantitatively understand the separation of metal catalysts, carbon impurities and aggregates from SWCNT dispersions. First, experimental methods on purification by centrifugation are summarized; next, the theoretical approach is outlined; and lastly, the model is applied to experimental data to get a general interpretation. The keys given for the sedimentation of nanoparticles with different shapes should be valuable for the design and scaling of separation processes in fluid suspensions.

2. Experimental methods

Unless otherwise specified, experimental data were extracted from previous publications [25–27]. Pristine SWCNT materials were either home-made [25,26] or purchased from Carbon Solutions Inc. (Riverside, CA, USA, AP-SWNT grade) [27]. In both cases, the synthesis was performed by the electric arc reactor. Pristine SWCNT powders contain abundant impurities, basically metal catalyst particles (nickel and yttrium), graphitic particles, and amorphous carbon. The average SWCNT diameter is approximately 1.5 nm, and nanotube lengths follow a log-normal distribution, whose median value is around 315 nm [6,28].

Pristine SWCNTs were sometimes modified by thermal treatment in air or hydrogen at different temperatures, acid reflux in HCl, HNO_3 or H_2SO_4, or chemical functionalization reactions using different precursors in the diazonium salts route [26,27].

In a typical experiment, pristine or modified SWCNTs were dispersed in a surfactant solution using an ultrasonic probe. The resulting dispersion was processed in one of the following centrifugation machines:

- Hermle Z383 (Hermle Labortechnik GmbH, Wehingen, Germany), using centrifugation vials of ~ 50 mL, which remain leaned by 27.3° during the whole process [25,26]. It was operated in the speed range of 3000 to 13,000 rpm, for a time interval of 30 min.
- Beckman Coulter L-100XP ultracentrifuge (Beckman Coulter Life Sciences, Indianapolis, IN, USA), with a SW55Ti 3671 rotor and 5 mL Beckman centrifugation tubes, which remain nearly perpendicular (90°) [27]. The rotational velocity was 31,400 r.p.m. (120,000 $\times g$) for 60 min.

It can be observed that both centrifugation machines have different rotor geometries. This fact will be taken into account for the mathematical modelling (Fig. 1). In all the cases, the supernatant dispersion is analyzed, while the sediment is discarded.

Two control parameters were utilized for monitoring the centrifugation process: the total mass yield (Y_c) and the SWCNT purity index (*PI*). Both parameters were determined by optical absorption spectroscopy in the visible-near infrared region.

The Y_c value is calculated as the ratio of the absorbance (optical thickness) at 850 nm of the dispersion before (A_0) and after (A_f) the centrifugation process. It is considered to be equal to the following relationship of nanoparticle concentrations:

$$Y_c = \left(\frac{A_f}{A_0}\right)_{\lambda=850\ nm} \approx \frac{[SWCNT]_f + [C_i]_f + [M]_f}{[SWCNT]_0 + [C_i]_0 + [M]_0} \quad (1)$$

where [SWCNT] is the mass concentration of SWCNTs, C_i refers to carbonaceous impurities, and M stands for metal catalyst nanoparticles (Ni and Y). The denominator $[SWCNT]_0 + [C_i]_0 + [M]_0$ is given by the initial solid weight, which is always known. The initial mass of the metal impurities ($[M]_0$) was calculated by thermogravimetric analysis (TGA) in oxidative atmospheres [25, 27]. The initial relative quantity of Ni and Y remains close to the original synthetic ratio (4/1 in atoms, i.e. 72,5% Ni and 27.5% Y referred to the total metal mass) [25,27].

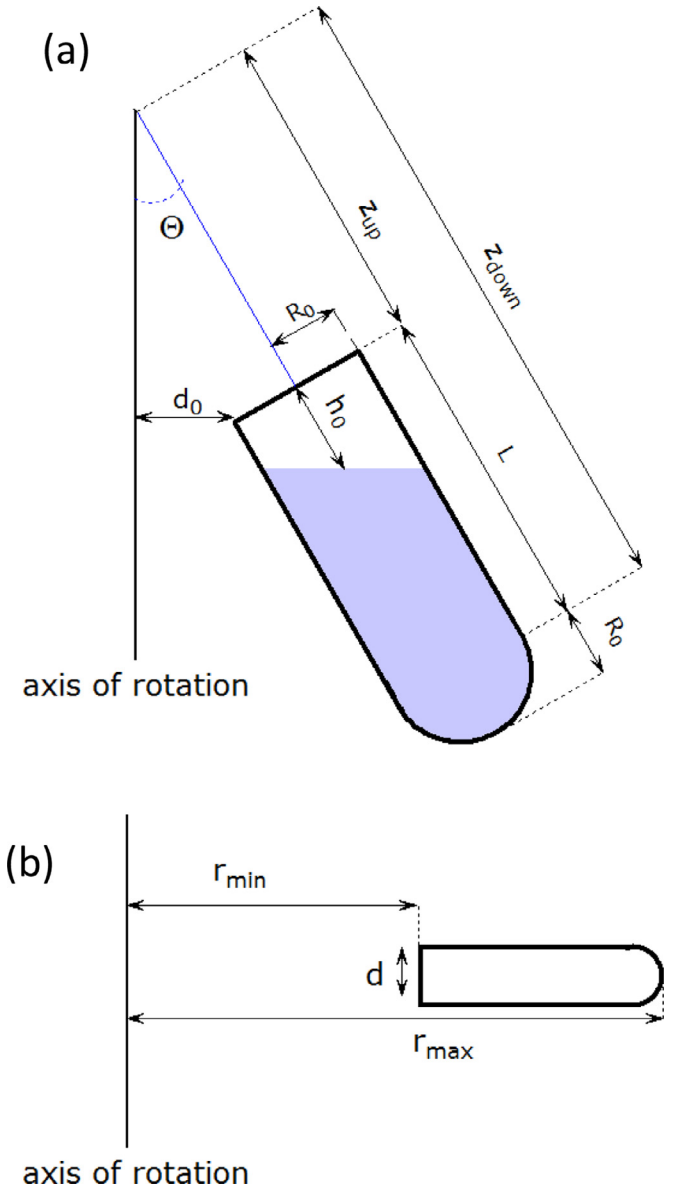

Fig. 1. Schematic diagrams showing parameters of the considered rotor geometries: a) Lateral section of a leaning vial in the Hermle Z383 machine, with position coordinates; b) Lateral section of a perpendicular vial in the Beckman Coulter SW55Ti rotor in motion.

The purity index (*PI*), which is expected to improve upon centrifugation, is calculated from the area of the spectral S_{22} band of SWCNTs [25–27]. The *PI* is the ratio between the background-subtracted peak area ($S_{22,p}$) and the total area under the peak ($S_{22,t}$). It is assumed to be related with the mass concentration of SWCNTs according to the relationship:

$$PI = \frac{S_{22,p}}{S_{22,t}} \approx 0.32 * \frac{[SWCNT]}{[SWCNT] + [C_i]} \quad (2)$$

where the coefficient 0.32 is considered as a good approximation for the *PI* of a pure SWCNT sample [29,30]. The *PI* was first rec-

ommended as a SWCNT purity control parameter using a linear background for the calculation of $S_{22,p}$ [31]. Later, it has been discussed that the model might be too simple, since the background is not really linear and *PI* values might not be reliable [30,32]. However, the original recommendation is here maintained for reasons of simplicity, and it will be demonstrated that calculations are in good agreement with experimental data under this assumption.

3. Theoretical approach

3.1. Coefficient of sedimentation

The most relevant parameters of centrifugation can be deduced from fundamental concepts in the context of non-equilibrium thermodynamics [33,34]. In the following, the k-subscript is used to indicate different components existing in the system (individual SWCNTs, SWCNT bundles, carbonaceous impurities, and metal catalyst particles). The sedimentation coefficient of the k-component (s_k) arises as the particle velocity (v_k) normalized by the centrifugal acceleration:

$$s_k = \frac{v_k}{\omega^2 r} \tag{3}$$

Where ω is the angular velocity and r the distance to the rotation axis. Applying the Svedberg equation [35,36] and the Stokes law (Section S1, Supporting Information), Eq. (3) can be transformed into:

$$s_k = \frac{M_k(1-\rho\upsilon_k)}{f_k} \tag{4}$$

Where M_k is the particle mass, ρ the density of the liquid mixture, υ_k the nanoparticle specific volume, and f_k the friction coefficient, which is related to the equivalent hydrodynamic radius through the Stokes equation:

$$f_k = 6\pi\eta R_{H:k} \tag{5}$$

where η is the viscosity of the liquid medium and $R_{H:k}$ stands for the hydrodynamic radius of k-particles. For a spherical particle, R_H is its radius. Explicit expressions have been worked out for other geometries, such as rod-like particles [37,38] or discs [21]. Here, SWCNTs are modelled as rigid cylinders [15,18], and the f coefficient is estimated as the orientation-averaged translational friction coefficient.

Precise estimations for the R_H of SWCNTs have been calculated by means of the boundary element method [37] or the path integral method [38]. Both methods consider different geometries (rectangular cylinder, rectangular open cylinder, sphero-cylinder) and provide coincident results for a large enough aspect ratio (r_p), which is defined as the ratio between nanotube length (L) and diameter (the relative deviation is less than 1% for $r_p \geq 10$). In this study, results have been computed from the formula given in [37]:

$$R_H = \frac{L}{2(lnr_p + \Gamma_t(r_p))} \tag{6}$$

where the shape function $\Gamma_t(r_p)$ corresponds to the one provided for the rectangular cylinder in Table 2 of [37]. Differences in geometry and method are irrelevant in the limit of very large r_p values. Indeed, the R_H value tends to:

$$\lim_{r_p \to \infty} R_H = \frac{L}{2\ ln\ r_p} \tag{7}$$

Certainly, SWCNTs exhibit an extreme r_p value (greater than 150). Still, we double-checked that our assumptions regarding geometry and method do not affect our results. In fact, the outcome does not significantly change when considering the sphero-cylinder case or applying the explicit functional form of R_H obtained from the path integral method.

3.2. Number fraction of nanoparticles in the supernatant dispersion

The remaining fraction of nanoparticles (X) with a given size and shape can be calculated as a function of s_k and the centrifugation parameters (speed and time). The fraction $X(s_k, \omega, t)$ also depends on the rotor geometry (Section S2, Supporting Information). In this article, two different rotor geometries are considered (Fig. 1), standing for both centrifugation machines already described in Section 2. In the most general case, only numerical solutions are possible for $X(s_k, \omega, t)$. When the system exhibits cylindrical symmetry (sector-shaped vial perpendicular to the rotation axis), the conservation of mass turns into the well-known Lamm equation [39], which allows for analytical solutions under certain limiting conditions (Section S2, Supporting Information) [40,41].

3.3. Influence of particle size distribution and SWCNT bundling

As above mentioned, the s coefficient of individual nanoparticles with a given shape and size can be calculated by Eq. (4). Subsequently, the $X(s_k, \omega, t)$ fraction of such definite particles can be calculated, as explained in Section 3.2. Now, the size distribution of those particles is taken into account. For the case of SWCNTs, a log-normal distribution (f_{ln}) of cylinder lengths and a fixed diameter D are assumed (Fig. 2.a and Supporting Information Section S3) [28]. Therefore, the fraction of SWCNTs in the supernatant, if all the SWCNTs were individualized, would be:

$$X_{SWCNT}(\omega, t) = \int_0^\infty X(s_{SWCNT}, \omega, t)\ f_{ln}(\mu_L, \sigma_L, L)\ dL \tag{8}$$

As D is assumed to be constant, an explicit dependence on D is omitted. Moreover, SWCNTs tend to aggregate, forming bundles with a number n of nanotubes. The bundle size can be represented by a surrounding cylinder with radius R_b [42]. The s coefficient is calculated by Eq. (4), where the bundle mass (M_b) is the sum of individual SWCNT masses. Typically, SWCNTs form a triangular packing network with N hexagonal layers, and a full layer contains $6N$ nanotubes. The R_b value is approximated by the radius of the enveloping cylinder (Fig. 2.b) [43]. The probability $P_b(n)$ of finding a bundle with n SWCNTs decreases exponentially with n [42]:

$$P_b(n) = \frac{e^{-\ n\ \xi}}{\sum_{m=1}^{\infty} e^{-\ m\ \xi}} \tag{9}$$

Where ξ is a fitting parameter modelling the bundle size (the larger ξ, the less number of nanotubes). The denominator ensures that the probability is normalized (the sum of the probabilities of all the possible values of the number of nanotubes must be 1). For a given value of ξ, the average number of nanotubes per bundle is:

$$n_b = \frac{\sum_{n=1}^{\infty} n e^{-\ n\ \xi}}{\sum_{m=1}^{\infty} e^{-\ m\ \xi}} = \frac{1}{1\ -\ e^{-\ \xi}} \tag{10}$$

The mass fraction of SWCNTs remaining in the supernatant is thus:

$$X_{SWCNT}(\omega, t) = \frac{\sum_{n=1}^{\infty} \int_0^\infty X(s_{SWCNT}, \omega, t)\ M_b(n, L)\ P_b(n,\ \mu_L, \sigma_L, L)\ dL}{\sum_{n=1}^{\infty} \int_0^\infty M_b(n, L)\ P_b(n,\ \mu_L, \sigma_L, L)\ dL} \tag{11}$$

$P_b(n, \mu_L, \sigma_L, L)$ being the probability density for a bundle comprising n nanotubes whose maximum length is L. The concentration (mass/volume) of SWCNTs under centrifugation can thus be written as:

$$[SWCNT](\omega,\ t) = N_{SWCNT,0} \sum_{n=1}^{\infty} \int_0^\infty X(s_{SWCNT}, \omega, t) M_b(n, L) P_b(n, \mu_L, \sigma_L, L) dL \tag{12}$$

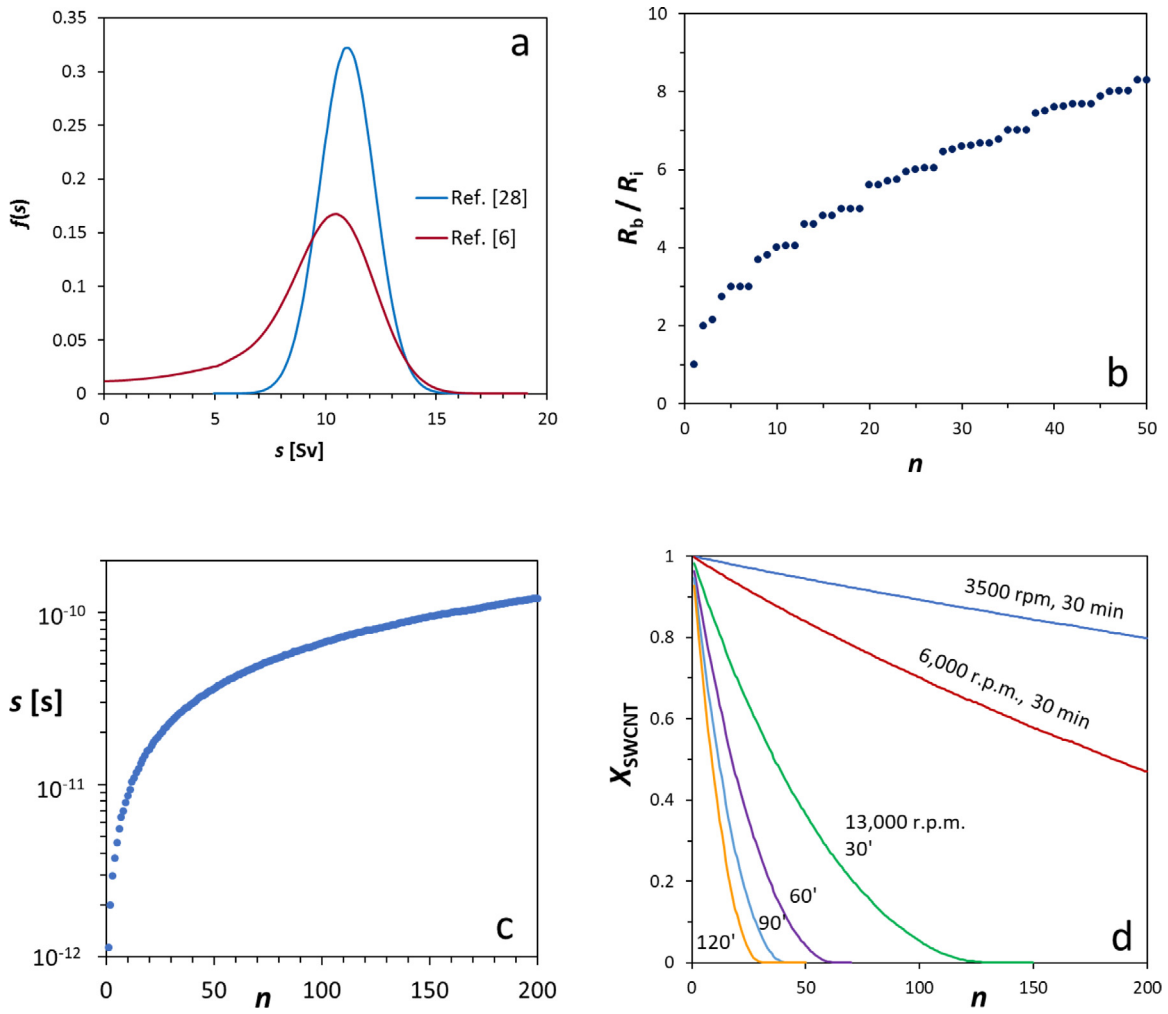

Fig. 2. The effect of size distribution and SWCNT bundling on sedimentation: a) Distribution of the *s* coefficient for arc-discharge SWCNT samples, assuming log-normal length distributions of individual SWCNTs [6,28]; b) Ratio between the bundle radius and the individual SWCNT radius (R_b / R_i) as a function of the *n* number of SWCNTs in the bundle; c) Average sedimentation coefficient (*s*) as a function of *n*; and d) Fraction of SWCNTs in the supernatant (X_{SWCNT}) for different centrifugation conditions, as a function of *n*.

where $N_{SWCNT,0}$ is the initial number of SWCNTs per volume unit. Further details are given in the Supporting Information (Section S4).

3.4. Selective sedimentation of impurities

Analogous expressions of (11) and (12) are worked out for other nanoparticles (carbonaceous impurities and metal particles). Their explicit forms are detailed in the Supporting Information (Section S5).

The size distribution of metal nanoparticles can be determined from transmission electron microscopy (TEM) images, where they are identified by their high contrast. The measured radii were fitted to a log-normal distribution, characterized by parameters $\mu_M = 1.167 \pm 0.186$ and $\sigma_M = 0.640 \pm 0.134$ (confidence intervals were estimated for a confidence level of 0.99). On the contrary, the size of carbonaceous impurities is elusive, and the associated log-normal parameters are considered as unknown variables.

The complete experimental data set is computed by a fitting procedure utilizing the algorithm of Levenberg–Marquardt [44]. The algorithm minimizes the modulus of a 9-component vector whose components are of the form:

$$g[i] = \frac{f_e(\omega,t)[i] - f_m(\omega,t)[i]}{f_m(\omega,t)[i]} \tag{13}$$

Table 1
The 9 magnitudes *f*[i] used to define the vector *g* considered for the fitting procedure (Eq. (13)) with data from Ref. [25].

f[i]	Type of function	Centrifugation conditions
f[1]	*Y*	$\omega = 3500$ rpm, $t = 30$ min
f[2]	*Y*	$\omega = 6000$ rpm, $t = 30$ min
f[3]	*Y*	$\omega = 13{,}000$ rpm, $t = 30$ min
f[4]	*PI*	$\omega = 0$, $t = 0$
f[5]	*PI*	$\omega = 3500$ rpm, $t = 30$ min
f[6]	*PI*	$\omega = 6000$ rpm, $t = 30$ min
f[7]	*PI*	$\omega = 13{,}000$ rpm, $t = 30$ min
f[8]	*[M]*	$\omega = 0$, $t = 0$
f[9]	*[M]*	$\omega = 13{,}000$ rpm, $t = 30$ min

Where f_e and f_m are, respectively, the estimated and measured values of the magnitudes described in Table 1. The objective of the fitting procedure is to minimize the value of:

$$\sum_{i=1}^{9} g[i]^2 \tag{14}$$

The fitting procedure considered 6 fitting parameters that are listed in Table 2.

Table 2
The six fitting parameters that were considered in the minimization algorithm (Equation 13) for the centrifugation of the SWCNT sample from Ref. [25].

Parameter	Estimated value	Units
Metal impurities		
μ_M	1.025[a]	Log (nm)
Carbonaceous impurities		
μ_R	0.698	Log (nm)
σ_R	0.8911921	Log (nm)
$[C_i]_0$	72.62219	Mass %
Carbon nanotubes		
$[SWCNT]_0$	8.838177	Mass %
ξ	0.06536317	–

[a] The estimated value of μ_M was obtained from the measured *Y* and *PI* values from Table 3. It is worthwhile to note that this value is within the confidence interval $\mu_M = 1.167 \pm 0.186$ obtained, in a completely independent way, from mere observations of transmission electron microscopy (TEM) images.

Table 3
Experimental data upon centrifugation of a SWCNT dispersion in leaned vials at different spin velocities for 30 min [25].

Sample dispersion	*Y* [%]	*PI*	$[M]_0$ [%][a]
Initial	100	0.034	13.87
3,500 rpm	79.3	0.044	–
6,000 rpm	61.5	0.058	–
13,000 rpm	25.5	0.071	9.75

[a] The initial quantity of metal impurities ($[M]_0$) is calculated from the TGA residue [25], transforming the metal oxide mass into the initial metal mass through a correction factor of 0.75 [27].

4. Results and discussion

For the leaning rotor geometry (Fig. 1.a), the integration of Eq. (11) indicates that nearly all individualized SWCNTs remain in the liquid dispersion under the considered centrifugation conditions. In fact, the *s* value of an individualized SWCNT is very low ($\sim 10^{-12}$ s = 10 Sv) [16], and the position *r* of a SWCNT is nearly unchanged after centrifugation at 13,000 r.p.m. (1,360 rad•s^{-1}) for 30-60 min (Equation S10, Supporting Information). For the ultracentrifugation in perpendicular vials (Figure 1.b), and assuming that SWCNT lengths follow the experimental log-normal distribution [28], the fraction of suspended SWCNTs is (Eq. S9): X_{SWCNT} ($\omega = 120{,}000 \times g$, $t = 1$h) = 0.867. Therefore, the fraction of settled individualized SWCNTs, being significant ($\sim$ 13%), is still minority. However, the rate of SWCNT sedimentation increases with bundling. Accordingly, Fig. 2 shows the *s* coefficient and the mass fraction in the supernatant dispersion (X_{SWCNT}) as a function of the bundle size (*n*).

4.1. The leaning rotor for low spin rates

First, the fitting procedure (Section 3.4) is applied to an experimental data set that was obtained upon centrifugation of a pristine SWCNT sample (Table 3). The outcome of the fitting procedure is summarized in Fig. 3 and Table 2. The estimated values approach to the experimental ones with relative deviations of < 5%. Logically, the concentration of the three nanoparticles (SWCNTs, carbonaceous impurities, metal catalysts) decreases upon centrifugation at increasing spin rates. The decrease in the SWCNT concentration is the slowest one, thus increasing the *PI* of the supernatant dispersion. The obtained ξ parameter (Table 2) indicates that the average number of SWCNTs in a bundle was of 16.3 in the initial dispersion, and decreased with centrifugation. For instance, it decreased to 12.6 after 30 min at 13,000 rpm. Some more details are given in the Supporting Information (Section S6). Despite the presence of the SDS surfactant and the utilization of ultrasounds to prepare the dispersion, many SWCNTs remained aggregated in relatively large bundles, decreasing its stability against sedimentation. Regarding carbonaceous impurities, the calculated median and average radius are 2 and 3 nm, respectively. The very small size of many carbonaceous impurities increases their stability in the colloid suspension and hinders their separation from SWCNTs in a single centrifugation process.

4.2. The effect of thermal oxidation

In the literature, thermal treatments under an air atmosphere have been applied as different stages of SWCNT purification processes [30,45–49]. Here, the treatment of pristine SWCNT powders at 350 °C for different times is considered [26].

At temperatures above 300 °C, oxygen rapidly reacts with carbon materials to give surface functional groups, which eventually evolve as CO and CO_2 gases, causing a loss of carbon mass [46,50,51]. Because of the carbon mass loss, encapsulated metal nanoparticles can be released and some impurities are detached from SWCNTs. Besides, metal catalysts are oxidized, at least in part or superficially, to give metal oxides, NiO and Y_2O_3 in this particular SWCNT sample. The total mass change (burn off) during the thermal treatment can be determined by direct weighing, while the mass of oxygen that remains on the treated carbon powder can be calculated from TGA and MS analysis (Section S7, Supporting Information).

In terms of SWCNT purification, direct effects of air oxidation mainly concern small amorphous carbon nanoparticles. Amorphous carbon is more reactive than graphite particles and SWCNTs, since oxygen more easily adsorbs on defect surface sites. Also, small nanoparticles exhibit the largest external surface and are preferentially oxidized. For modelling purposes, it is considered that both the gained oxygen and lost carbon are proportional to the particle surface, while it is assumed that the particle density does not change during the thermal treatment. Besides, an analogous model is applied to SWCNT bundles (Section 7, Supporting Information). The loss of mass of a bundle, assumed proportional to its surface, is modelled by the burning of external nanotubes.

Starting from a log-normal size distribution of spherical carbon impurities, the resulting distribution after the thermal treatment is not exactly log-normal (Fig. 4.a). Spherical nanoparticles with radius smaller than a threshold value (R_{th}) are simply burnt off, and the remaining ones experience a decrease in their radius. The oxidative process drastically reduces the weight of small nanoparticles, thus increasing the proportion of big impurities. Since big impurities are highly sensitive to sedimentation, the centrifugation of thermally treated samples leads to very high purities (*PI* values) of SWCNTs (Fig. 4.b).

Fig. 4.b includes experimental burnt-off mass and *PI* values (before and after centrifugation) of various SWCNT samples that were treated at 350 °C for different times between 0.5 and 4h. Burn-off data can be fitted to a function type A[1-exp(-B•*t*)], while the *PI* data set is fitted to a second order polynomial. The *PI* after centrifugation was calculated from the *PI* before centrifugation and the burn-off mass, and the theoretical values were compared with the experimental ones. To calculate the *PI* values after centrifugation we first computed the initial concentration of nanotubes and carbonaceous impurities from the *PI* values and metal concentrations before centrifugation (values at $t = 0$). Then, burn-off measures are used to estimate the resulting distributions of nanotubes and impurities (details can be found in Section 7, Supporting Information). Subsequently, we computed the resulting concentrations after centrifugation using Eq. (12) for nanotubes and the analogous one for impurities; this result yields the estimated *PI* values af-

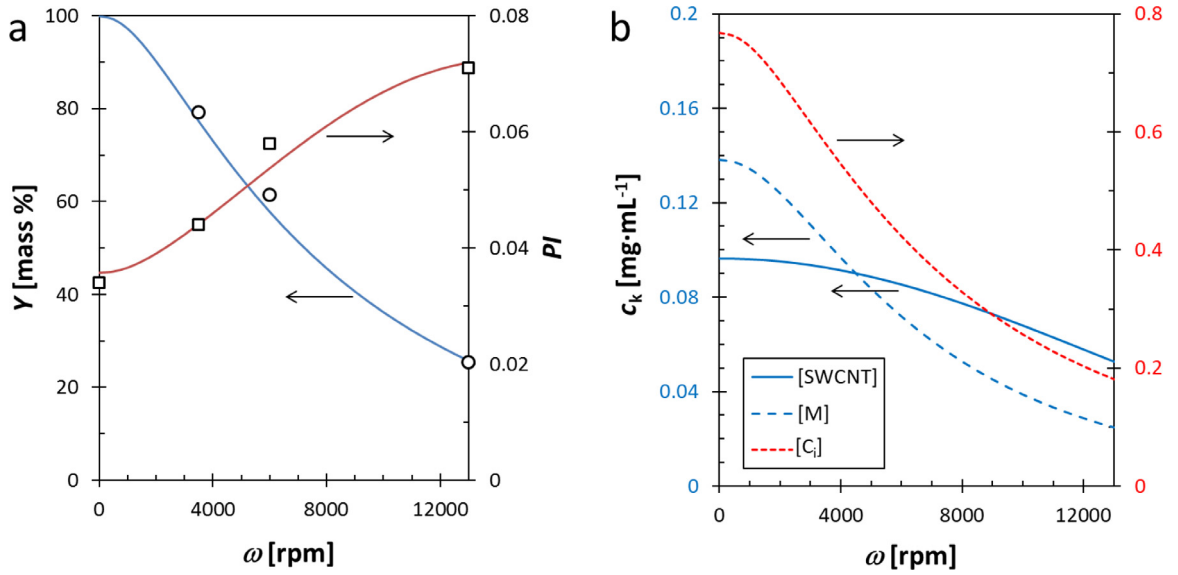

Fig. 3. Outcome of the fitting procedure on the centrifugation of pristine SWCNTs in the leaned rotor (data from Table 3): a) Experimental (circles and squares) and modelled centrifugation yields (*Y*) and purity indexes (*PI*) at different spin velocities; b) Modelled concentrations of SWCNTs, carbonaceous impurities, and metal nanoparticles for different spin velocities (initial total concentration is 1 mg mL^{-1}).

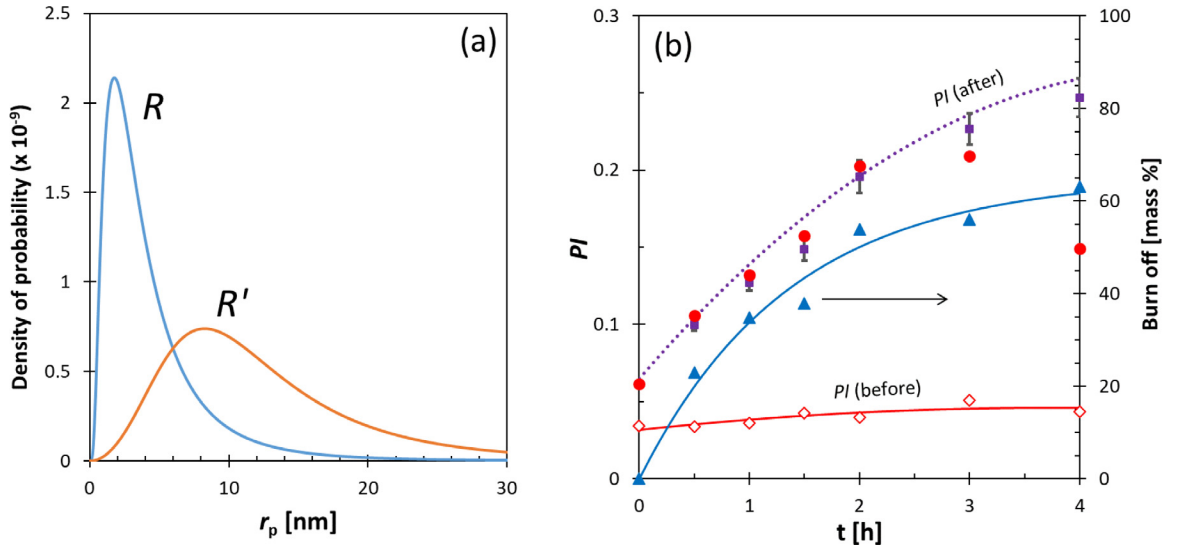

Fig. 4. Modelling results of thermal treatments in air: a) Calculated change in the size distribution (from the initial radius *R* to the final *R*') of spherical carbonaceous particles upon treatment at 350 °C for 2h; b) Evolution of the purity index (*PI*) of SWCNT samples treated at 350 °C for different times, before and after centrifugation at 13,000 rpm. The right axis (blue triangles and blue line) indicates the burnt-off material during the thermal treatment. Red diamonds and the red line are experimental *PI* data before centrifugation and the associated second order fitting line. Red circles are experimental *PI* data after centrifugation at 13,000 rpm. Purple squares and the purple dotted line are the *PI* values and trend line calculated with the model.

ter centrifugation. Purple squares in Fig. 4.b stand for the individually calculated values (i.e., values obtained taking as input data the measured values of *PI* and burn-off), and the purple dotted line was calculated from the respective trend functions (respectively, red and blue continuous lines). It was assumed that metal impurities totally transform into metal oxides. As-calculated *PI* values very well agree with experimental results (red dots in Fig. 4.b) for oxidation times of $t < 3$h. At longer times, experimental *PI* values are much lower than expected by the model, indicating that prolonged thermal treatments may induce agglomeration of the surviving SWCNTs.

The ξ parameter describing the SWCNT bundle size becomes higher than that previously found for the non-oxidized sample (Table 3). The new ξ value is associated with bundles in the range of 10-14 SWCNTs. The decrease in the bundle size after the oxidative treatment can be associated to the burning of SWCNTs and to the presence of hydrophilic oxygenated groups on the surface of SWCNTs, which facilitate the dispersion of SWCNTs into small bundles, increasing their stability [25].

The theory of sedimentation clearly suggests and supports that the elimination of small carbonaceous nanoparticles during thermal oxidative treatments is a key contribution to achieve the highest *PI* values after subsequent centrifugation of SWCNT suspensions. Besides, both the generation of small size debris and the aggregation of SWCNTs has to be avoided. Apparently, this effect is not efficiently achieved by other oxidative treatments in the liquid phase (reflux in HNO_3) and other gasification treatments (H_2 at 700 °C) [26].

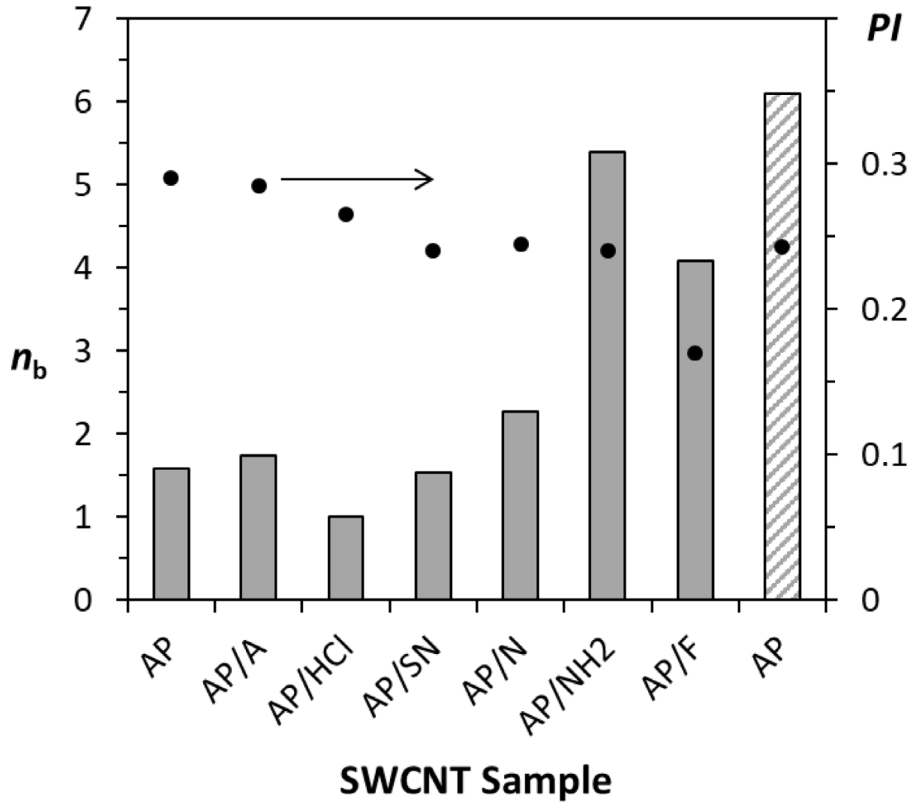

Fig. 5. Calculated average number of nanotubes in a bundle (n_b, bars) and experimental purity indexes after centrifugation (*PI*, black dots) for a series of pristine, treated and functionalized SWCNTs. Solid bars indicate refer to ultracentrifugation experiments while the weaved bar indicates the control experiment at a lower speed in the leaned rotor. Sample nomenclature: AP = pristine SWCNTs; AP/A = AP thermally treated in air; AP/HCl = AP/A treated in HCl reflux; AP/SN = AP/A treated in H_2SO_4/HNO_3 reflux; AP/N = AP treated in HNO_3 reflux; AP/NH2 = AP functionalized with $-C_6H_4CH_2NH_2$ groups; and AP/F = AP functionalized with $-C_6H_4(CF_2)_7CF_3$ groups [27].

4.3. Ultracentrifugation in the rotor geometry with perpendicular vials

The behavior of SWCNTs upon ultracentrifugation at 31,400 rpm in a perpendicular rotor geometry was studied on pristine SWCNTs and after different pretreatments of oxidation and chemical functionalization [27]. In all the cases, the *PI* value substantially improved after centrifugation; the ratio $PI(\omega,t)/PI_0$ was in the range of 1.7 to 3.0. Multiple mechanisms might contribute to the colloidal stability of SWCNTs and the differential sedimentation of impurities. Here, we will try to conceptualize quantitatively the main acting factors, which appear to be mostly related to nanoparticle aggregation, in particular to the SWCNT bundle size.

The starting hypothesis remains that, even after the differential functionalization treatments, all the SWCNT samples can be modelled by three parameters (μ_L, σ_L, ξ). The concentration of SWCNTs before and after the centrifugation treatment can be approximately determined:

$$\frac{[\mathrm{SWCNT}]_f}{[\mathrm{SWCNT}]_0} = Y_c \frac{PI_f\ (1-[\mathrm{M}]_f)}{PI_0\ (1-[\mathrm{M}]_0)} \tag{15}$$

Where the metal concentration ([M]) is given as a mass ratio. Therefore, the model algorithm provides a fitting value for ξ, which is associated to the average number of nanotubes in a bundle (n_b).

Fig. 5 shows the calculated n_b value for the series of SWCNT samples. By means of alternative calculations, it was confirmed that contributions such as the mass of functional groups and possible inaccuracies in metal determinations have only a minor influence. It is noteworthy that the n_b number is in the range of 1-2 nanotubes for most of the samples that were processed by high speed centrifugation. In particular, it is around 1-2 for pristine (AP), air-oxidized (AP/A), and air-oxidized/acid treated (AP/HCl, AP/SN) SWCNT samples. The direct nitric acid treatment (AP/N) induces a certain degree of aggregation, while n_b reaches 4-5 for the covalently functionalized samples (AP/NH2, AP/F). Certainly, severe nitric acid treatments and covalent functionalization can induce aggregation through specific interactions between functional groups [45,52]. Besides, functionalization treatments may change the absorbance spectrum, which is the basis of the *PI* calculation [27].

With the aim of getting a direct comparison with previous Sections 3.1 and 3.2, we performed an additional centrifugation experiment in the leaned rotor (13,000 rpm, 30 min) using a dispersion of 1 mg/mL AP-SWCNT in 5 mg/mL SDBS. The *PI* and Y_c values resulted to be 0.243 and 23.6%. Accordingly, it can be calculated a n_b value in the range of 3.0–8.3, most typically around 6.1 (Fig. 5). For an identical SWCNT sample, the n_b value resulting from high speed centrifugation is lower than the calculated after low speed centrifugation. This result indicates an improved degree of SWCNT individualization with ultracentrifugation, as it was previously suggested by Cathcart and Coleman [5]. The individualization cannot be only explained by the sedimentation of aggregates, and its origin remains unclear.

Conclusions

The separation of various nanoparticle types (here, tubes and spheres) by centrifugation mainly depends on differences in their sedimentation coefficient. The degree of aggregation, including SWCNT bundling, and breakage, substantially change the *s* coefficient and the sedimentation rate. The centrifugation experiments can be well modelled by a mathematical algorithm based on the

rotor geometry, nanoparticle geometry, and fundamental equations of sedimentation. The model qualitatively supports the following conclusions:

(a) The sedimentation coefficient (*s*) of individual nanotubes is substantially lower than that of solid spheres. This fact allows a selective sedimentation, even under a certain degree of nanotube bundling.
(b) Oxidative thermal treatments in air improve the separation of nanotubes through the selective elimination of the smallest spherical carbon particles, which have small *s* values and are otherwise difficult to separate.
(c) Ultracentrifugation allows an improved separation of individual SWCNTs. However, the mechanism that facilitates the unzipping of SWCNT bundles into individual nanotubes at high centrifugation speeds is still unclear.
(d) Chemical functionalization causes only minor changes in the *s* coefficient through small variations in the specific volume and the dragging factor (*f*). Indirectly, the presence of hydrophilic groups might facilitate the dispersion of SWCNTs in aqueous media, decreasing the *s* coefficient. However, physicochemical treatments might also induce aggregation or break the structures into even smaller particles. These combined facts well explain the behavior of SWCNT suspensions after different pretreatments, in good quantitative agreement with classical centrifugation theories. Moreover, these findings are of general character and can be easily transferred to centrifugation processes involving nanoparticles of different types and shapes, thus contributing a more efficient preparation of corresponding suspensions or inks with improved properties.

Declaration of Competing Interest

The authors declare that they have no known competing financial interests or personal relationships that could have appeared to influence the work reported in this paper.

Acknowledgements

Financial support from Spanish MICINN/AEI under project PID2019-104272RB-C51/AEI/10.13039/501100011033 and the Diputación General de Aragón under project T03_20R (*Grupo Reconocido*) is acknowledged.

Supplementary materials

Supplementary material associated with this article can be found, in the online version, at doi:10.1016/j.cartre.2021.100084.

References

[1] H. Hu, A. Yu, E. Kim, B. Zhao, M.E. Itkis, E. Bekyarova, Influence of zeta potential on dispersability and purification of single-walled carbon nanotubes, J. Phys. Chem. B 109 (2005) 11520–11524, doi:10.1021/jp050781w.
[2] A. Yu, E. Bekyarova, M.E. Itkis, D. Fakhrutdinov, R. Weber, R.H. Haddon, Application of centrifugation to the large-scale purification of electric-arc produced single-walled carbon nanotubes, J. Am. Chem. Soc. 128 (2006) 9902–9908, doi:10.1021/ja062041m.
[3] P. Vichchulada, J. Shim, M.D. Lay, Non-oxydizing purification method for large volumes of long undamaged single-walled carbon nanotubes, J. Phys. Chem. C 112 (2008) 19186–19192, doi:10.1021/jp803989d.
[4] N.P. Bhatt, P. Vichchulada, M.D. Lay, Bulk purification and deposition methods for selective enrichment in high aspect ratio single-walled carbon nanotubes, J. Am. Chem. Soc. 134 (2012) 9352–9361, doi:10.1021/ja302136x.
[5] H. Cathcart, J.N. Coleman, Quantitative comparison of ultracentrifuged and diluted single-walled carbon nanotube dispersions, Chem. Phys. Lett. 474 (2009) 122–126, doi:10.1016/j.cplett.2009.04.022.
[6] A.J. Blanch, C.E. Lenehan, J.S. Quinton, Parametric analysis of sonication and centrifugation variables for dispersion of single walled carbon nanotubes in aqueous solutions of sodium dodecylbenzene sulfonate, Carbon 49 (2011) 5213–5218, doi:10.1016/j.carbon.2011.07.039.
[7] M.S. Arnold, S.I. Stupp, M.C. Hersam, Enrichment of single-walled carbon nanotubes by diameter in density gradients, Nano Lett. 5 (2005) 713–718, doi:10.1021/nl050133o.
[8] M.S. Arnold, A.A. Green, J.F. Hulvat, S.I. Stupp, M.C. Hersam, Sorting carbon nanotubes by electronic structure using density differentiation, Nature Nanotech. 1 (2006) 60–65, doi:10.1038/nnano.2006.52.
[9] J.A. Fagan, M.L. Becker, J. Chun, P. Nie, B.A. Bauer, J.R. Simpson, A. Hight-Walker, E.K. Hobbie, Centrifugal length separation of carbon nanotubes, Langmuir 24 (2008) 13880–13889, doi:10.1021/la801388a.
[10] K. Yanagi, Y. Miyata, H. Kataura, Optical and conductive characteristics of metallic single-wall carbon nanotubes with three basic colors: cyan, magenta, and yellow, Appl. Phys. Express 1 (2008) 0340031–0340033, doi:10.1143/APEX.1.034003.
[11] A.A. Green, M.C. Hersam, Colored semitransparent conductive coatings consisting of monodisperse metallic single-walled carbon nanotubes, Nano Lett. 8 (2008) 1417–1422, doi:10.1021/nl080302f.
[12] F. Bonaccorso, T. Hasan, P.H. Tan, C. Sciascia, G. Privitera, G. Di Marco, P.G. Gucciardi, A.C. Ferrari, Density gradient ultracentrifugation of nanotubes: interplay of bundling and surfactants encapsulation, J. Phys. Chem. C 114 (2010) 17267–17285, doi:10.1021/jp1030174.
[13] A.A. Green, M.C. Hersam, Nearly single-chirality single-walled carbon nanotubes produced via orthogonal iterative density gradient ultracentrifugation, Adv. Mater. 23 (2011) 2185–2190, doi:10.1002/adma.201100034.
[14] Y. Kuang, J. Liu, X. Sun, Ultrashort single-walled carbon nanotubes: density gradient separation, optical property, and mathematical modeling study, J. Phys. Chem. C 116 (2012) 24770–24776, doi:10.1021/jp3028337.
[15] M.S. Arnold, J. Suntivich, S.I. Stupp, M.C. Hersam, Hydrodynamic characterization of surfactant encapsulated carbon nanotubes using analytical ultracentrifuge, ACS Nano 2 (2008) 2291–2300, doi:10.1021/nn800512t.
[16] C. Backes, E. Karabudak, C.D. Schmidt, F. Hauke, A. Hirsch, W. Wohlleben, Determination of the surfactant density on SWCNTs by analytical ultracentrifugation, Chem. Eur. J. 16 (2010) 13176–13184, doi:10.1002/chem.200903461.
[17] J.A. Fagan, M. Zheng, V. Rastogi, J.R Simpson, C.Y. Khripin, C.A. Silvera Batista, A.R. Hight Walker, Analyzing surfactant structures on length and chirality resolved (6,5) single-wall carbon nanotubes by analytical ultracentrifugation, ACS Nano 7 (2013) 3373–3387, doi:10.1021/nn4002165.
[18] C.A. Silvera Batista, M. Zheng, C.Y. Khripin, X. Tu, J.A. Fagan, Rod hydrodynamics and length distributions of single-wall carbon nanotubes using analytical ultracentrifugation, Langmuir 30 (2014) 4895–4904, doi:10.1021/la404892k.
[19] J. Walter, K. Löhr, E. Karabudak, W. Reis, J. Mikhael, W. Peukert, W. Wohlleben, H. Cölfen, Multidimensional analysis of nanoparticles with highly disperse properties using multiwavelength analytical ultracentrifugation, ACS Nano 8 (2014) 8871–8886, doi:10.1021/nn503205k.
[20] S. Lam, M. Zheng, J.A. Fagan, Characterizing the effect of salt and surfactant concentration on the counterion atmosphere around surfactant stabilized SWCNTs using analytical ultracentrifugation, Langmuir 32 (2016) 3926–3936, doi:10.1021/acs.langmuir.6b00605.
[21] J. Walter, T.J. Nacken, C. Damm, T. Thajudeen, S. Eigler, W. Peukert, Determination of the lateral dimension of graphene oxide nanosheets using analytical ultracentrifugation, Small 11 (2015) 814–825, doi:10.1002/smll.201401940.
[22] T.J. Nacken, C.E. Halbig, S.E. Wawra, C. Damm, S. Romeis, J. Walter, M.J. Tehrani, Y. Hu, Y. Ishii, S. Eigler, W. Peukert, Structural factors controlling size reduction of graphene oxide in liquid processing, Carbon 125 (2017) 360–369, doi:10.1016/j.carbon.2017.09.066.
[23] S.P. Ogilvie, M.J. Large, M.A. O'Mara, P.J. Lynch, C.L. Lee, A.A.K. King, C. Backes, A.B. Dalton, Size selection of liquid-exfoliated 2D nanosheets, 2D Mater 6 (2019) 031002, doi:10.1088/2053-1583/ab0dc3.
[24] C. Backes, D. Campi, B.M. Szydlowska, K. Synnatschke, E. Ojala, F. Rashvand, A. Harvey, A. Griffin, Z. Sofer, N. Marzari, J.N. Coleman, D.D. O'Regan, Equipartition of energy defines the size-thickness relationship in liquid-exfoliated nanosheets, ACS Nano 13 (2019) 7050–7061, doi:10.1021/acsnano.9b02234.
[25] A. Ansón-Casaos, J.M. González-Domínguez, M.T. Martínez, Separation of single-walled carbon nanotubes from graphite by centrifugation in a surfactant or in polymer solutions, Carbon 48 (2010) 2917–2924, doi:10.1016/j.carbon.2010.04.028.
[26] A. Ansón-Casaos, M. González, J.M. González-Domínguez, M.T. Martínez, Influence of air oxidation on the surfactant-assisted purification of single-walled carbon nanotubes, Langmuir 27 (2011) 7192–7198, doi:10.1021/la200730k.
[27] A. Ansón-Casaos, J.M. González-Domínguez, I. Lafragüeta, J.A. Carrodeguas, M.T. Martínez, Optical absorption response of chemically modified single-walled carbon nanotubes upon ultracentrifugation in various dispersants, Carbon 66 (2014) 105–118, doi:10.1016/j.carbon.2013.08.048.
[28] A. Ansón-Casaos, J.C. Ciria, O. Sanahuja, S. Víctor-Román, J.M. González-Domínguez, E. García-Bordejé, A.M. Benito, W.K. Maser, The viscosity of dilute carbon nanotube (1D) and graphene oxide (2D) nanofluids, Phys. Chem. Chem. Phys. 22 (2020) 11474–11484, doi:10.1039/d0cp00468e.
[29] B.J. Landi, H.J. Ruf, J.J. Worman, R.P. Raffaelle, Effects of alkyl amide solvents on the dispersion of single-wall carbon nanotubes, J. Phys. Chem. B 108 (2004) 17089, doi:10.1021/jp047521j.
[30] B.J. Landi, H.J. Ruf, C.M. Evans, C.D. Cress, R.P. Raffaelle, Purity assessment of single-wall carbon nanotubes, using optical absorption spectroscopy, J. Phys. Chem. B 109 (2005) 9952–9965, doi:10.1021/jp044990c.
[31] M.E. Itkis, D.E. Perea, R. Jung, S. Niyogi, R.C. Haddon, Comparison of analytical techniques for purity evaluation of single-walled carbon nanotubes, J. Am. Chem. Soc. 127 (2005) 3439–3448, doi:10.1021/ja043061w.

[32] A.V. Naumov, S. Ghosh, D.A. Tsyboulski, S.M. Bachilo, R.B. Weisman, Analyzing absorption backgrounds in single-walled carbon nanotube spectra, ACS Nano 5 (2005) 1639–1648, doi:10.1021/nn1035922.
[33] L.D. Landau, E.M. Lifshitz, Fluid Mechanics, Pergamon Press, 1959.
[34] S.R. De Groot, P. Mazur, Non-Equilibrium Thermodynamics, Courier Corporation, 2013.
[35] T. Svedberg, H. Rinde, The ultracentrifuge, a new instrument for the determination of size and distribution of size of particle and amicroscopic colloids, J. Am. Chem. Soc. 46 (1924) 2677–2693, doi:10.1021/ja01677a011.
[36] T. Svedberg, K.O. Pedersen, The Ultracentrifuge, Oxford University Press, London, England, 1940.
[37] S.R. Aragon, D. Flamik, High precision transport properties of cylinders by the boundary element method, Macromolecules 42 (2009) 6290–6299, doi:10.1021/ma900453c.
[38] M.L. Mansfield, J.F. Douglas, Transport properties of rod-like particles, Macromolecules 41 (2008) 5422–5432, doi:10.1021/ma702839w.
[39] O. Lamm, Die differentialgleichung der ultrazentrifugierung, Arkiv för Matematik, Astronomi och Fysik 21b (2) (1929) 1–4.
[40] J.W. Williams, K.E. Van Holde, R.L. Baldwin, H. Fujita, Chem. Rev. 58 (1958) 715–744, doi:10.1021/cr50022a005.
[41] W.L. Archibald, The integration of the differential equation of the centrifuge, Ann. N. Y. Acad. Sci. 43 (1942) 211–227, doi:10.1111/j.1749-6632.1942.tb57151.x.
[42] A.N.G. Parra-Vasquez, J.G. Duque, M.J. Green, M. Pasquali, Assessment of length and bundle distribution of dilute single-walled carbon nanotubes by viscosity measurements, AIChE J. 60 (2014) 1499–1508, doi:10.1002/aic.14325.
[43] A. Peigney, Ch. Laurent, E. Flahaut, R.R. Bacsa, A. Rousset, Specific surface area of carbon nanotubes and bundles of carbon nanotubes, Carbon 39 (2001) 507–514, doi:10.1016/S0008-6223(00)00155-X.
[44] D.W. Marquadt, An algorithm for least squares estimation of nonlinear parameters, SIAM J. Appl. Math. 11 (1963) 431–441, doi:10.1137/0111030.
[45] M.T. Martinez, M.A. Callejas, A.M. Benito, M. Cochet, T. Seeger, A. Ansón, J. Schreiber, C. Gordon, C. Marhic, O. Chauvet, J.L.G. Fierro, W.K. maser, Sensitivity of single wall carbon nanotubes to oxidative processing: structural modification, intercalation and functionalization, Carbon 41 (2003) 2247–2256, doi:10.1016/S0008-6223(03)00250-1.
[46] F. Picó, J.M. Rojo, M.L. Sanjuán, A. Ansón, A.M. Benito, M.A. Callejas, W.K. Maser, M.T. Martínez, Single-walled carbon nanotubes as electrodes in supercapacitors, J. Electrochem. Soc. 151 (2004) A831–A837, doi:10.1149/1.1738678.
[47] A.G. Ryabenko, T.V. Dorofeeva, G.I. Zvereva, UV-VIS-NIR spectroscopy study of sensitivity of single-wall carbon nanotubes to chemical processing and Vander-Waals SWNT/SWNT interaction. Verification of the SWNT content measurements by absorption spectroscopy, Carbon 42 (2004) 1523–1535, doi:10.1016/j.carbon.2004.02.005.
[48] J. Li, Y. Zhang, A simple purification for single-walled carbon nanotubes, Physica E 28 (2005) 309–312, doi:10.1016/j.physe.2005.03.022.
[49] N. Dementev, S. Osswald, Y. Gogotsi, E. Borguet, Purification of carbon nanotubes by dynamic oxidation in air, J. Mater. Chem 19 (2009) 7904–7908, doi:10.1039/B910217E.
[50] I.W. Chiang, B.E. Brinson, R.E. Smalley, J.L. Margrave, R.H. Hauge, Purification and characterization of single-wall carbon nanotubes, J. Phys. Chem. B 105 (2001) 1157–1161, doi:10.1021/jp003453z.
[51] I.W. Chiang, B.E. Brinson, A.Y. Huang, P.A. Willis, M.J. Bronikowski, J.L. Margrave, R.E. Smalley, R.H. Hauge, Purification and characterization of single-wall carbon nanotubes (SWNTs) obtained from the gas-phase decomposition of CO (HiPco process), J. Phys. Chem. B 105 (2001) 8297–8301, doi:10.1021/jp0114891.
[52] A. Ansón-Casaos, J.M. González-Domínguez, A.M. Díez-Pascual, M.A. Gómez-Fatou, M.T. Martínez, Choosing the chemical route for carbon nanotube integration in poly(vinylidene fluoride), J. Phys. Chem. C 116 (2012) 16217–16225, doi:10.1021/jp302212m.